



Separating He II and Si XI Emission Components in Off-limb 304 Å Observations

Ivan Loboda¹ · Anton Reva¹ · Sergey Bogachev¹ · Alexey Kirichenko¹ · Artem Ulyanov¹

Received: 5 July 2023 / Accepted: 8 November 2023 / Published online: 22 November 2023
© The Author(s), under exclusive licence to Springer Nature B.V. 2023

Abstract

Solar extreme ultraviolet (EUV) imaging instruments usually have a channel centered at 304 Å to observe the strong He II 303.8 Å line, which is valuable for studying the dynamics of chromospheric and transition-region structures. In off-limb regions where He II is weak, however, the coronal Si XI 303.3 Å line becomes significant and provides a background haze that reduces the contrast of He II structures such as jets and macrospicules, complicating the interpretation of the observations. Generally, the separation of this background would require spectroscopic observations. In this article, we take an alternate approach by reconstructing the differential emission measure (DEM) of the quiescent corona to obtain synthetic radial emission profiles in the Si XI 303.3 Å line and show that at altitudes above 20 Mm it makes the major contribution to the background. We also find the silicon abundance to be significantly, by around 80%, lower in the quiet Sun than in the coronal hole. Based on the DEM profiles, we propose a physical model for the off-limb radial intensity profile in the Si XI 303.3 Å line. The model's main advantage is the possibility to estimate and subtract the background of the quiescent corona using observations in the 304 Å channel alone, which may be of use for future studies of small-scale solar activity.

Keywords Corona, quiet · Corona, models · Spectrum, ultraviolet · Spectral line, intensity and diagnostics

1. Introduction

Observations of the Sun in the extreme ultraviolet (EUV) spectral range provide extensive information about active phenomena in the solar atmosphere, starting with their largest forms, such as solar flares, coronal mass ejections, and prominences (e.g. Reva et al., 2016; Reva, Ulyanov, and Kuzin, 2016; Reva et al., 2017; Seaton and Darnel, 2018; Mierla et al., 2022) and down to small-scale activity, including micro- and nanoflares, coronal jets, and coronal bright points (e.g. Joulin et al., 2016; Kirichenko and Bogachev, 2017; Ulyanov et al., 2019; Kumar et al., 2019; Bogachev et al., 2020). One of the most well-established

✉ I. Loboda
ivan.loboda@cosmos.ru

¹ Space Research Institute of the Russian Academy of Sciences, Moscow, Russia

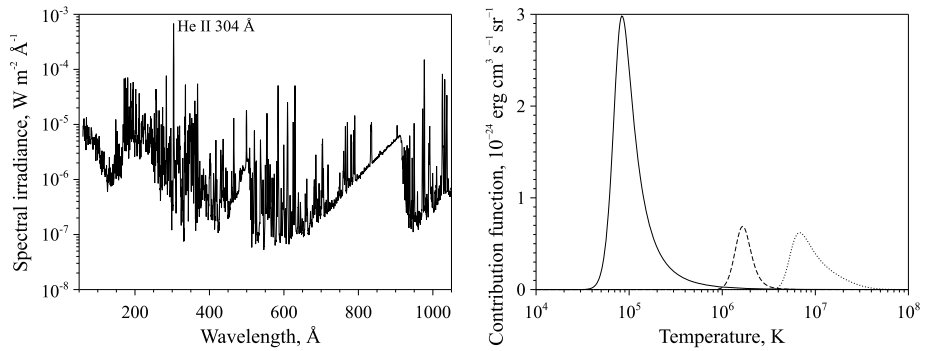


Figure 1 *Left:* averaged spectrum of the full solar disk in the EUV range obtained by the SDO/EVE spectrograph (Woods et al., 2012). *Right:* contribution functions for the He II 303.8 Å (solid line), Si XI 303.3 Å (dashed line), and Ca XVIII 302.2 Å (dotted line) spectral lines provided by the CHIANTI database (Del Zanna et al., 2021). Contribution function for the Ca XVIII 302.2 Å line has been scaled up by a factor of 100 for illustrative purposes.

approaches for such observations, along with the use of classical slit spectrographs and spectroheliographs, is the method of spectroscopic imaging (also often referred to as imaging spectroscopy) comprising observations of the solar disk and corona over a wide field of view, performed simultaneously in several narrow (on the order of several or tens of Å) spectral channels centered around a number of bright emission lines (e.g. Holman, 2016).

One of the spectral channels most widely used in such studies is the 304 Å channel, centered near the resonance Ly α line of a singly ionized helium atom at 303.8 Å – the brightest solar emission line in the EUV range (Figure 1, left panel). This line is formed at temperatures of around 8×10^4 K (Figure 1, right panel), and therefore the 304 Å channel is most commonly used to study the structure and dynamics of the upper chromosphere and transition region. At the same time, this is probably one of the most difficult EUV channels to interpret. Unlike other commonly observed EUV emission lines, primarily that of the highly ionized iron atoms in the corona, the solar plasma is optically thick in the He II 303.8 Å line due to the combination of its strength and the relatively high density of the chromosphere and transition region. In addition, the effects of nonequilibrium ionization, resonant scattering, resonant photoexcitation, and the photoionization–recombination mechanism make a significant contribution to the formation of this spectral line (Jordan et al., 1993; Labrosse and Gouttebroze, 2001; Andretta, Del Zanna, and Jordan, 2003; Pietarila and Judge, 2004; Golding, Leenaarts, and Carlsson, 2017; Del Zanna et al., 2020) and should be considered, often through detailed inverse modeling, to correctly estimate plasma parameters from such observations.

Apart from the effects listed above, which already significantly complicate the interpretation of observations in the 304 Å channel compared to other EUV bands, an additional difficulty is posed by the presence of closely spaced Si XI 303.3 Å and Ca XVIII 302.2 Å spectral lines within the typical bandwidth of this channel. These lines are formed at significantly different temperatures with only insignificant overlap in their contribution functions (Figure 1, right panel) and thus reflect different structures in the solar atmosphere, which are then superimposed in the same image. Whereas the Ca XVIII 302.2 Å line is formed at high temperatures of around 7 MK and thus is only observed in solar flares, the Si XI 303.3 Å line is formed at around 1.6 MK, which is close to the temperature of the quiescent corona, and therefore the background signal from this line is inevitably present in 304 Å images.

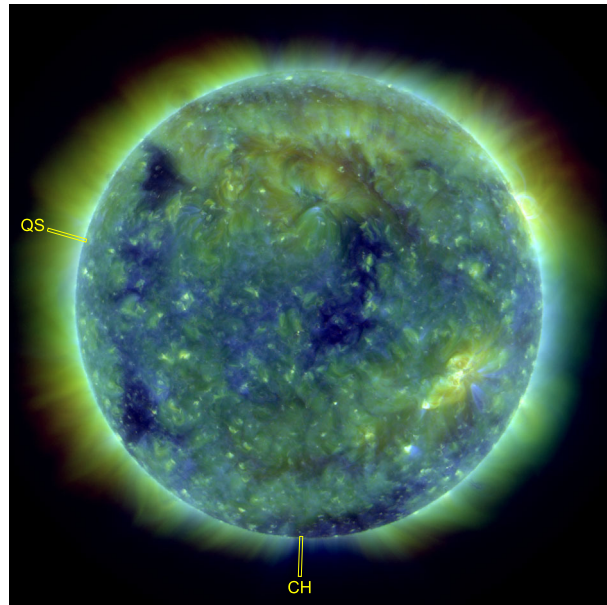
When interpreting such observations, it is customary to assume that the contribution from the Si XI 303.3 Å line is insignificant, and thus the observations in the 304 Å channel reflect predominantly the structures of the thin but complex and dynamic transition region between the chromosphere and the solar corona. This assumption is largely justified for on-disk observations far from active regions and is supported by spectroscopic observations (Cushman and Rense, 1978; Del Zanna and Andretta, 2011; Del Zanna et al., 2015; Parker and Kankelborg, 2022). However, when observing active regions and, especially, off-limb regions of the lower corona, the contribution from the Si XI 303.3 Å line to the total radiation flux in the 304 Å channel becomes significant and even predominant (Thomas and Neupert, 1994; Thompson and Brekke, 2000; Andretta, Telloni, and Del Zanna, 2012), which makes it necessary to separate the background signal of He II and Si XI ions for such observations.

In addition to a more complicated interpretation of observations, especially when performed quantitatively (e.g. Loboda and Bogachev, 2015, 2017), blending of the He II and Si XI lines in the 304 Å channel obstructs the identification of faint transition-region structures against the coronal background. These include macrospicules and other types of EUV jets (e.g. Kiss, Gyenge, and Erdélyi, 2017; Kiss and Erdélyi, 2018; Loboda and Bogachev, 2019; Liu et al., 2023), as well as small-scale prominences observed off-limb (e.g. Labrosse, Dalla, and Marshall, 2010; Loboda and Bogachev, 2015). To increase the contrast of observations in the lower corona, various empirical models for background normalization or subtraction are often employed, which, however, rarely have a physical basis.

The most reliable method to isolate the He II 303.8 Å and Si XI 303.3 Å lines would be based, of course, on spectroscopic observations. Its practical application, however, is significantly limited. In addition to the high spectral resolution required for such observations, spectroscopic instruments typically have a limited field of view compared to the solar angular dimensions, a long-slit scanning time across the field of view, and, in general, a relatively small number of such observations available, which, in turn, requires a coordinated observation programme for each object of study. The most recent instrument capable of such observations was the *Coronal Diagnostic Spectrometer* (CDS: Harrison et al., 1995) onboard the *Solar and Heliospheric Observatory* (SOHO: Domingo, Fleck, and Poland, 1995), which stopped its operation in 2014. As part of the dedicated observational campaign, it was used to obtain monochromatic images of the full solar disk independently in the He II 304 Å and Si XI 303.3 Å lines, which showed the dominance of the Si XI radiation in the off-limb regions of the corona, as well as its significant contribution near active regions (Thompson and Brekke, 2000). However, such estimates are more of a qualitative nature and are of little use for other observations in the 304 Å channel.

In this work, we study the possibility of separating the background signals of the He II 303.8 Å and Si XI 303.3 Å lines in off-limb observations using only telescopic images obtained in several EUV passbands to reconstruct the differential emission measure (DEM) of the quiescent corona. Based on the results obtained, we propose and give a physical basis for a model of the background intensity in the Si XI 303.3 Å line, the parameters of which can be estimated using observations in the 304 Å channel alone. In Section 2, we give a brief description of the observational data used and methods for their numerical processing. In Section 3, we present the results obtained, and on their basis we propose a model for the off-limb intensity profile in this line. We then discuss the significance of these results for further studies of the solar transition region and conclude with a brief summary in Section 4.

Figure 2 Location of the radial slits in the quiet-Sun region (*QS*) and in the polar coronal hole (*CH*) against the composite image from the SDO/AIA's 211 Å (red channel, 2 MK), 193 Å (green channel, 1.2 MK), and 171 Å (blue channel, 0.6 MK) filters recorded at 03:00 UT.



2. Data and Methods

To obtain the background intensity of the Si XI 303.3 Å line without using spectroscopic observations, we rely on the reconstruction of the differential emission measure (DEM) in the off-limb regions of the quiescent corona. The best opportunity for this is provided by the *Atmospheric Imaging Assembly* (AIA: Lemen et al., 2012) of the *Solar Dynamics Observatory* (SDO: Pesnell, Thompson, and Chamberlin, 2012), which regularly observes the full solar disk and the lower corona with high spatial and temporal resolution simultaneously in seven spectral channels, which, apart from the 304 Å channel, include the 94 Å, 131 Å, 171 Å, 193 Å, 211 Å, and 335 Å channels, covering the wide temperature range from 0.6 MK (171 Å channel) to 10–20 MK (131 Å and 193 Å channels).

For our analysis, we have chosen the period from 00:00 to 06:00 UT on 13 May 2010, at the very beginning of the regular operations of SDO. This was done primarily to eliminate the effects of gradual degradation of the optical elements and the detectors of the telescopes over time (Boerner et al., 2014), which occurs unevenly in different spectral channels and thus can significantly distort the results of the consequent DEM analysis. In addition, the proximity of this observation period to the deep solar minimum of 2008–2009 ensures a smaller number of large-scale manifestations of solar activity, such as active regions or prominences, that would significantly reduce the observable portion of the quiescent corona.

First, we identified a number of small regions in the off-limb parts of the AIA images that were distant from large-scale solar activity and free from significant inhomogeneities, formed by persistent large-scale coronal structures, such as plumes or helmet streamers. We then placed narrow radial slits in two of these regions, characterized by significantly different temperature conditions in the corona: one in the quiet-Sun region close to the Equator and another in the southern polar coronal hole. The locations of the slits are indicated in Figure 2. Within each of the slits, off-limb radial intensity profiles were obtained in all of AIA's EUV channels, starting from the limb and up to a radial distance of 120 Mm, where intensity

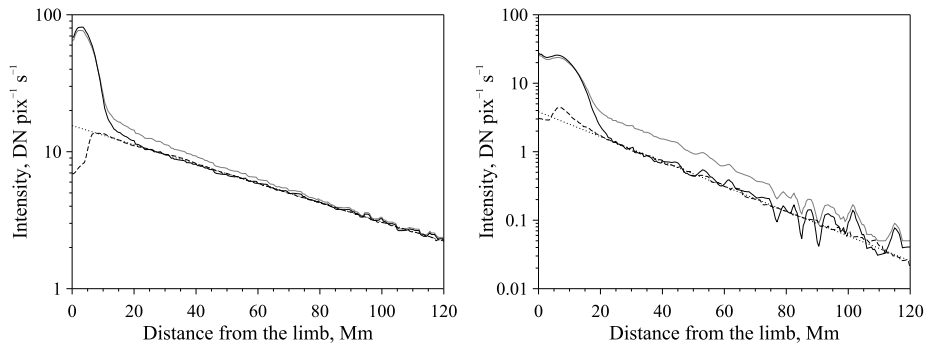


Figure 3 Radial intensity profiles of the undisturbed corona (*solid gray lines*) in the 304 \AA channel observed in the quiet-Sun region (*left*) and in the polar coronal hole (*right*). Intensity profiles corrected for the scattered light are *solid black lines*, the synthesized intensity profiles of the Si XI 303.3 \AA line are *dashed lines*, and their fit with the proposed model are *dotted lines*.

becomes close to the noise levels, and with a step of 500 km, roughly corresponding to the angular resolution of the AIA.

Even in the absence of large-scale solar activity, a significant number of small-scale transient phenomena – primarily macrospicules and larger types of EUV jets – are still present in the lower corona. Their typical lifetime is about 15–30 minutes (Pucci et al., 2013; Kiss, Gyenge, and Erdélyi, 2017; Loboda and Bogachev, 2019), and therefore, given a sufficiently long observation period (six hours in our case), it is possible to eliminate such structures with a low-pass temporal filter. To obtain the intensity of the undisturbed corona at each point of the radial profiles, we obtained a corresponding time series from the whole observational sequence and then calculated the median signal. The resulting off-limb radial intensity profiles of the undisturbed corona are shown in Figure 3.

Another effect that can influence our analysis is instrumental – the scattered light from the bright emission of the solar disk, which can be significant close to the limb. For AIA’s EUV channels, semiempirical point spread functions (PSF) have been estimated by Poduval et al. (2013). However, the deconvolution procedure required to eliminate the scattered-light component in each image is extremely computationally intensive, which makes it practically inapplicable for large datasets. At the same time, scattered light in the off-limb regions is predominantly defined by the average intensity of the adjacent part of the solar disk, and thus is not likely to fluctuate significantly with time. To estimate the scattered-light intensity in the examined regions of the corona, we have therefore performed the convolution in a sufficiently large vicinity of these regions just for the first, central, and last images in the dataset and then took the average.

We have thus found that in the 304 \AA channel the scattered-light intensity reaches its maximum of $2.7 \text{ DN pix}^{-1} \text{ s}^{-1}$ at around 15 Mm above the limb in the quiet-Sun region and of $1.5 \text{ DN pix}^{-1} \text{ s}^{-1}$ at around 20 Mm in the coronal hole, making up to 15 and 40% of the recorded signal, respectively, and thus having a nonnegligible effect on the obtained results (Figure 3). Above that height, it gradually decreases in an exponential manner and can be fit with a smooth function at larger heights to eliminate noise at low intensity levels. The relative intensity of scattered light is, however, much smaller in other EUV channels of AIA, being most prominent in the 171 \AA and 131 \AA bands (up to 7–7.5% at 30 Mm) and almost insignificant in other channels (below 1–2%). We thus believe that its effect on the obtained DEM profiles is on the order of several percent as well and thus is comparable to the inversion method’s error.

For each point of the obtained radial profiles, we reconstructed the DEM of the coronal plasma using the sparse-inversion method proposed and implemented by Cheung et al. (2015). The main disadvantage of this method is its tendency to overestimate the high-temperature component of the DEM at above 15 MK, which effect can be eliminated by the additional use of observations in the soft X-ray range, for example those obtained with the *X-Ray Telescope* (XRT: Golub et al., 2007) of the *Hinode* mission (Kosugi et al., 2007). For the quiescent corona, however, with its temperature typically not exceeding 2 MK, this method is expected to give reliable results without the need for additional observations. Indeed, the subsequently obtained DEMs have no significant component above 3 MK at all examined locations. Moreover, this implies that there is no detectable contribution from the Ca XVIII 302.2 Å line to the observed intensities, and thus it can be safely excluded from further consideration.

Combined with the contribution function for the Si XI 303.3 Å line, typical silicon abundance in the corona, and the effective area of the AIA's 304 Å channel, the obtained DEM profiles allowed us to reconstruct the synthetic radial-intensity profiles of this optically thin line. The contribution function was calculated using the CHIANTI atomic database (Del Zanna et al., 2021) and is shown in the right panel of Figure 1. At the same time, obtaining the synthetic intensity profiles of the optically thick He II 303.8 Å resonance line would be a much more difficult task, requiring detailed handling of radiative transfer and, correspondingly, knowledge of the ion-density distribution along the line of sight. However, due to the absence of other strong lines within the passband of the 304 Å channel, it can be reliably assumed that nearly all of the residual radiation in this channel is due to the He II line, and therefore the synthetic profile of the Si XI line alone would be enough to separate the background signal of the two ions. Beyond that, the obtained DEM profiles allowed us to examine the thermal structure of the corona by calculating the DEM-weighted average temperature at each point of the radial profiles, which we use for the subsequent analysis.

3. Results and Discussion

After having obtained the synthetic radial profiles of the Si XI 303.3 Å line, we found that at heights above 20 Mm, they closely match in their quasi-exponential shape the intensity profiles of the total radiation in the 304 Å channel, but with a certain scaling factor. At the same time, we expect the intensity of the He II 303.8 Å line to decrease quickly with height due to the sharp temperature rise at the base of the corona and the shift of helium ionization balance to full ionization. We thus find it reasonable to assume that nearly all of the radiation in the 304 Å channel above 20 Mm comes from the Si XI ion alone. In this paradigm the main reason for the apparent scaling of Si XI synthetic profiles should be the choice of the typical silicon abundance value used in their reconstruction.

By setting the silicon abundance to 2.3×10^{-5} (or 7.36 on the commonly used logarithmic scale) in the quiet-Sun region and to 1.1×10^{-4} (8.04) in the coronal hole, we could achieve a nearly perfect match of the Si XI synthetic profiles with the observed 304 Å signal above 20 Mm (Figure 3). These abundance values are respectively significantly lower and significantly higher than the commonly used (e.g. in CHIANTI) coronal silicon abundance of around $(7.1 - 7.3) \times 10^{-5}$ (7.86–7.87; Fludra and Schmelz, 1999; Schmelz et al., 2012). At the same time, the value for the quiet Sun is close to the photospheric abundance of $(3.2 - 3.3) \times 10^{-5}$ (7.51–7.52; Grevesse, Asplund, and Sauval, 2007; Asplund et al., 2009; Lodders, Palme, and Gail, 2009), whereas the value for the coronal hole is close to 1.26×10^{-4} (8.10) obtained by Feldman et al. (1992) and Feldman and Laming (2000).

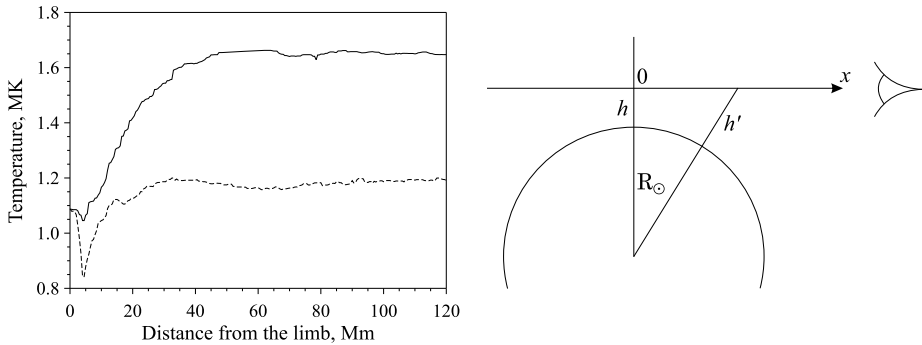


Figure 4 *Left:* radial temperature profiles obtained from the DEM profiles in the quiet-Sun region (*solid line*) and in the coronal hole (*dashed line*). *Right:* a schematic for determining the local distance from the photosphere h' along the line of sight x at a given tangent distance from the limb h . R_{\odot} is the solar radius.

This leads us to the idea that such an approach can also be used as a simple but efficient tool for silicon-abundance estimates in the absence of spectroscopic observations.

At the lower heights – up to 10 Mm in the quiet-Sun regions and up to 15 Mm in coronal holes – the background signal in the 304 Å channel is, in turn, dominated by the He II emission. Most of this radiation is formed in the outer shell of numerous chromospheric structures – primarily spicules and small macrospicules, which are continuously present at the limb and therefore cannot be eliminated by the median filter (Section 2). The above difference in the height of transition from helium- to silicon-dominated radiation (i.e. from chromospheric and transition-region structures to the corona) thus reflects the greater average height of spicules and macrospicules observed in coronal holes (Pereira, De Pontieu, and Carlsson, 2012; Bogachev et al., 2022).

Generally, the obtained synthetic Si XI 303.3 Å intensity profiles already solve the problem of separating the background signal of He II and Si XI ions in the 304 Å channel, although the use of the DEM reconstruction method may be viewed as somewhat inconvenient and computationally expensive and moreover requires the availability of multiwavelength observations. At the same time, the obtained radial DEM profiles allow us to draw further conclusions about the nature of the off-limb intensity profiles in the Si XI 303.3 Å line by analyzing the thermal structure of the lower corona.

The radial temperature profiles that were obtained from the DEM profiles for the quiet-Sun region and for the coronal hole are shown in the left panel of Figure 4. Apart from the nonphysical temperature jump near the limb, where the DEM calculation is least reliable due to significant and wavelength-dependent photoionization absorption by the chromospheric structures, primarily spicules, both temperature profiles show similar behavior, with a relatively fast temperature increase in the lower corona up to heights of about 20–30 Mm above the limb, after which the profiles stabilize near a certain constant level, around 1.65 MK in the quiet-Sun region and around 1.2 MK in the coronal hole.

Although these temperature profiles are effectively a DEM-weighted average along the line of sight, from the considerations of symmetry we can assume that individual radial temperature profiles should also follow a similar pattern and reach a constant level at heights not exceeding 20–30 Mm above the photosphere. Such behavior would be in good agreement with existing semiempirical models of the solar chromosphere and lower corona based on spectroscopic observations, such as the widely used VAL-IIIC model (Vernazza, Avrett, and Loeser, 1981) and its later developments, based on the more recent observational data

(Avrett and Loeser, 2008). In these models a sharp increase in temperature takes place in the transition region at altitudes of about 2–3 Mm, after which the temperature profile becomes significantly flatter and reaches a constant level of around 1.5 MK at altitudes above 10–20 Mm.

Of course, more accurate estimates of coronal temperatures would be provided by spectroscopic observations of multiple coronal lines, whereas DEM reconstructions depend both on instrument calibrations and model imperfections. Whereas some of such studies show a very good correspondence with our results (e.g. Landi, Feldman, and Dere (2002) obtained a temperature of 1.35 MK at 20 Mm above the limb for a quiet-Sun region), others show significantly lower temperatures (Warren and Brooks (2009) obtained an average temperature of 1.1 MK at 40–60 Mm above limb), which can be explained, at least in part, by different choices of observation time, location, and spectral range. What is important, however, is that both of these studies indicate a nearly isothermal composition of plasma along the line of sight. From geometry considerations, again, we can assume that the temperature is constant above these heights.

Furthermore, some studies have found the temperature to be less than 1 MK in coronal holes, from either hydrostatic fits to the electron-density profiles (Wilhelm et al., 1998) or with line-ratio diagnostics (David et al., 1998). This can be explained by the presence of some higher-temperature plasma from the quiet-Sun corona along the line of sight due to the relatively small size of the coronal hole or, again, by the varying conditions for different observations. At the same time, DeForest et al. (1997) estimated the temperature in a polar plume to be in between 1.0 and 1.5 MK from observed Fe ionization states, whereas hydrostatic temperature profiles modeled by Pascoe, Smyrli, and Van Doorselaere (2019) based on the off-limb EUV intensity profiles reach a constant level of 1.4 MK in the quiet Sun and 1.2 MK in the coronal hole, which is more consistent with our estimates.

Given such temperature profiles, we can assume the temperature to be constant above the height of around 20 Mm, which allows us to derive an analytical expression for the radial profile of the electron density n_e . In the isothermal case, it can be expressed, along with the total density of the corona, as

$$n_e(h) \approx n_p(h) = n_0 e^{-(h-h_0)/H}, \quad (1)$$

where h is the height above the limb, n_0 is the density at some reference height h_0 , and H is the scale height, defined as $H = k_B T / m_p g$, where k_B is the Boltzmann constant, T is the temperature, m_p is the mass of a proton, and g is the acceleration of gravity.

The electron-density profile, in turn, defines how the emission measure (EM) changes with the distance from the limb, since the latter is defined as an integral of n_e^2 over the line of sight:

$$\text{EM}(h) = \int_{-\infty}^{\infty} n_e^2 dx = n_0^2 \int_{-\infty}^{\infty} e^{-2(h'-h_0)/H} dx, \quad (2)$$

where $h' = \sqrt{(h + R_\odot)^2 + x^2} - R_\odot$ is the distance from the photosphere at a certain point x along the line of sight, with the origin being the closest point to the center of the Sun (see the schematic in the right panel of Figure 4), and R_\odot is the solar radius. In this analysis, we also assume spherical symmetry in the close vicinity of the examined regions of the quiescent corona, which is partly justified by the fact that we have deliberately chosen for our analysis the most homogeneous regions of the corona as possible.

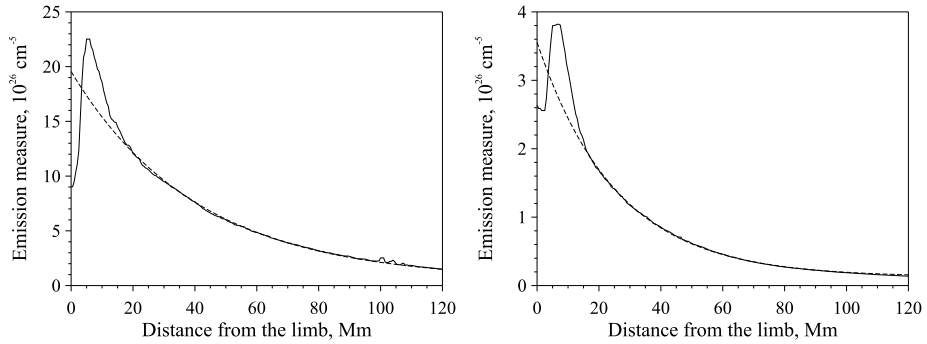


Figure 5 Radial profiles of the emission measure (solid line) obtained from the DEM profiles in the quiet-Sun region (left) and in the coronal hole (right). Dashed line shows the fit to these profiles with the proposed model function.

Since in our study only the lower part of the corona is considered (up to a distance of 120 Mm above the limb), we can assume that $h \ll R_{\odot}$. Furthermore, the rapid decrease of density with height due to the relatively small scale height of about 50–70 Mm compared to the size of the Sun allows us to assume that the main contribution to the integral in Equation 2 is given by a small region near the origin, and therefore only the small values of x ($x \ll R_{\odot}$) are relevant. With these two assumptions, we can consider that $h' \approx h + \frac{x^2}{2(R_{\odot}+h)}$, which significantly simplifies Equation 2 and gives an explicit expression for the EM radial profile:

$$\begin{aligned}
 EM(h) &\approx n_0^2 e^{-2(h-h_0)/H} \int_{-\infty}^{\infty} e^{-x^2/(R_{\odot}+h)H} dx = \\
 &= n_0^2 e^{-2(h-h_0)/H} \sqrt{\pi(R_{\odot}+h)H}. \tag{3}
 \end{aligned}$$

Data-based radial profiles of the EM can be obtained from the previously calculated DEM profiles by summing over the temperature. The result of this operation for the examined regions of the undisturbed corona is shown in Figure 5. In these plots the EM profiles have been additionally fitted with the model function from Equation 3. We can thus see that the proposed model is in extremely good agreement with observations at altitudes above 20 Mm, where the isothermal condition has been previously assumed for the corona. In our case the scale height obtained from these fits was found to be 70 Mm for the quiet-Sun region and 50 Mm for the coronal hole, which corresponds to coronal temperatures of 1.8 MK and 1.3 MK, respectively.

These temperature values are somewhat higher than those previously obtained directly from the DEM profiles, with the discrepancy, however, not exceeding 10%, which we consider to be good accuracy, given the estimated error of AIA’s initial calibration on the order of 25% (Boerner et al., 2012), as well as possible imperfections of the DEM reconstruction method for a relatively small number of partly correlated spectral channels. On the other hand, these discrepancies can also be accounted for by the fact that our model is purely hydrostatic and does not consider the nonzero radial velocity in the lower corona, on the order of 10 km s^{-1} , which corresponds to the initial phase of solar-wind acceleration and would lead to a steeper decrease of density with height. Finally, our model does not account

for the change in the acceleration of gravity with height, with the opposite effect on density profiles.

To be of practical use, the proposed model should be related to the observed quantity – the signal in the 304 Å images. Luckily, in the isothermal case the observed intensity I in the Si XI 303.3 Å line is directly proportional to the EM:

$$I(h) = \int_0^{\infty} G(T) \text{DEM}(T) dT \approx G(T_{\text{cor}}) \text{EM} = I_0 e^{-2(h-h_0)/H} \sqrt{\pi(R_{\odot} + h)H}, \quad (4)$$

where $G(T)$ is the contribution function for this line, T_{cor} is the temperature of the corona, and I_0 is a scaling factor determined at an arbitrarily chosen height h_0 . The fits with this model function to the radial intensity profiles are shown in Figure 3, which also demonstrate excellent agreement with observations at heights above 10–20 Mm.

From the practical point of view, it is important that this model is defined by just two fitting parameters, the previously determined scale height H and the scaling factor I_0 . Taking into account that in the absence of small-scale transient phenomena, such as EUV jets, almost all the observed intensity at altitudes above 20 Mm is formed by the Si XI 303.3 Å line, it is possible to estimate the parameters of this model directly from observations in the 304 Å channel alone, without the need for a larger number of EUV channels that would be necessary for the correct reconstruction of the DEM profiles.

This significantly expands the possibilities of the proposed model, which can be applied to observations from a multitude of other instruments with a more limited set of EUV channels. First of all, these include the widely used *Extreme-ultraviolet Imaging Telescope* (EIT: Delaboudinière et al., 1995) of SOHO and the *Extreme Ultraviolet Imager* (EUVI: Wuelser et al., 2004) onboard the two *Solar Terrestrial Relations Observatory* (STEREO) spacecraft, which perform regular observations in four EUV channels – 171 Å, 195 Å, 284 Å, and 304 Å. Even more so, this model will be relevant to the data from the TESIS telescopes on the CORONAS-Photon spacecraft (Kuzin et al., 2009) and the *Extreme Ultraviolet Imager* (EUI: Rochus et al., 2020) of the recently launched *Solar Orbiter* mission (Müller et al., 2020), which conduct observations only in the 171 Å and 304 Å channels, or to the lower-resolution observations of the *Solar Ultraviolet Imager* (SUVI: Tadikonda et al., 2019) on the *Geostationary Operational Environmental Satellites* (GOES) and the *Solar Upper Transition Region Imager* (SUTRI: Bai et al., 2023) onboard the recently launched SATech-01 spacecraft. Finally, it will certainly be of use for a number of future EUV imagers, such as the ARKA small explorer mission (Kuzin et al., 2011) and the KORTES instrument for the *International Space Station* (Kirichenko et al., 2021).

An example of background subtraction with the proposed model is given in Figure 6. In its upper panel, showing the original image, the diffuse radiation of the corona is clearly visible, which significantly lowers the contrast of the transition-region jet-like structures observed in the He II 303.8 Å line. After applying the median filter and correcting for the scattered light, the resulting radial intensity profiles were individually fitted with the model function from Equation 4. Owing to the smoothness of the coronal background, the obtained approximations and their fitting parameters are also sufficiently smooth in the limbward (horizontal) direction. Together with the scattered-light estimate, such an intensity map can be used to eliminate the off-limb coronal background in the 304 Å images above around 15 Mm. In the lower panel of Figure 6, the background subtraction was made for all altitudes above the limb for better visual presentation, although it has no physical meaning below that height.

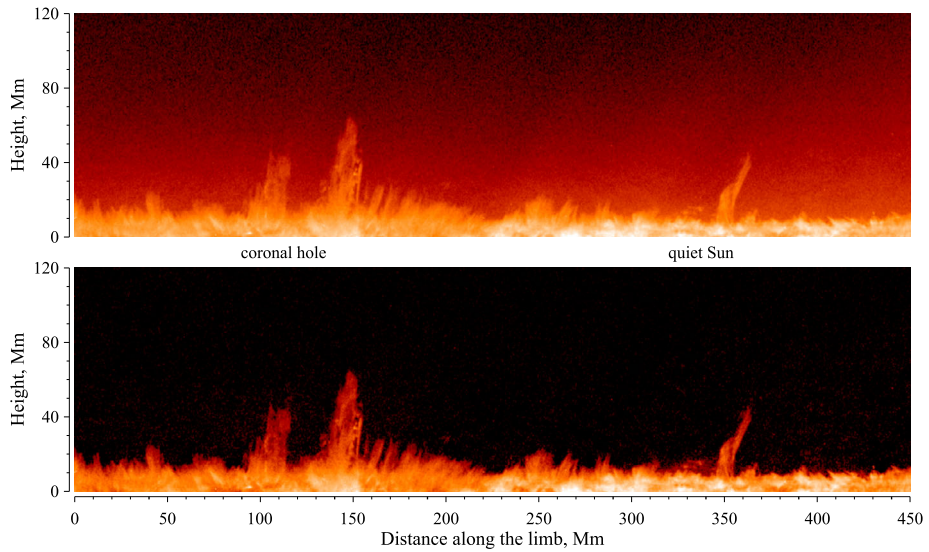


Figure 6 An example showing the elimination of coronal background from the SDO/AIA 304 Å image in the vicinity of a coronal-hole boundary: the original image (*top panel*) and the result of background subtraction (*bottom panel*). The intensity is in a logarithmic scale for visual clarity, with the lower intensity threshold of $5 \text{ DN pix}^{-1} \text{ s}^{-1}$ applied to constrain the contrast. A polar transformation of the off-limb region of the image was performed to simplify data processing and presentation.

Figure 6 also shows that in practice the proposed model provides a good approximation for the off-limb coronal background even in the areas where our assumption of spherical symmetry does not properly hold due to the presence of coronal structures, such as plumes and helmet streamers, or due to the proximity of active regions, thus leading to more complicated radial profiles of temperature and EM of the corona. It is also worth noting that the right-hand term in Equation 4 is slowly changing compared to the quickly decreasing exponent. This means that in many practical applications, which do not require high accuracy of background subtraction (e.g. to increase the contrast of observations), an even simpler, purely exponential model for the background signal can be used. Moreover, in such cases the computationally intensive correction for the scattered light may be also avoided, as the uncorrected intensity profiles have a similar exponential behavior, as illustrated by Figure 3.

4. Summary

In this work, we reconstructed the radial profiles of the DEM in two regions of the unperturbed solar corona: one in the quiet Sun and another in a polar coronal hole. With their help, synthetic radiation profiles were obtained for the Si XI 303.3 Å line. It was shown that the background radiation of the corona in the 304 Å channel at altitudes above 20 Mm is formed almost entirely by the Si XI line, whereas at lower heights the radiation of the resonant He II 303.8 Å line is dominant. Based on the analysis of the radial temperature profiles of the corona, a simple analytical model for the intensity of the Si XI 303.3 Å line as a function of height was proposed. Importantly, the parameters of this model can be estimated using observations in the 304 Å channel alone, which opens broad prospects for its practical

use in processing the observations from a multitude of existing and prospective EUV telescopes, as it provides a significant increase in contrast and simplifies the interpretation of such observations.

Overall, the procedure for removing the Si XI coronal background in the off-limb regions of 304 Å images can be summarized as the following sequence:

- i) Choose an observation period longer than the typical lifetime of chromospheric and transition-region structures (15–30 minutes) but significantly shorter than the solar rotation period (about 27 days).
- ii) Obtain the intensity of the undisturbed corona in the region of interest with the median (or any other low-pass) temporal filter.
- iii) Calculate the scattered-light intensity using PSF from Poduval et al. (2013) for a small number of images and subtract the average from the undisturbed-corona intensity obtained in the previous step (optional).
- iv) Fit individual radial profiles with the model function from Equation 4 (or with its exponential part only) using I_0 and H as the fitting parameters. Apply smoothing in the limbward direction if necessary.
- v) Subtract the resulting intensity map from the off-limb part of the images.

Acknowledgments We gratefully acknowledge the use of data from the SDO/AIA, the CHIANTI database, and the DEM inversion code by Cheung et al. (2015). SDO is a mission for NASA's Living With a Star (LWS) program. The data from the SDO/AIA are provided by the Joint Science Operations Center (JSOC) at Stanford University. CHIANTI is a collaborative project involving George Mason University, the University of Michigan (USA), University of Cambridge (UK), and NASA Goddard Space Flight Center (USA). We also thank the anonymous reviewer for carefully reading the manuscript and for useful suggestions, which helped to significantly improve our work and the clarity of its presentation.

Author contributions I. Loboda and A. Reva wrote the main manuscript text. A. Kirichenko obtained the observational data and performed its initial processing. I. Loboda and A. Ulyanov performed DEM reconstruction and obtained synthetic intensity profiles. A. Reva and S. Bogachev prepared the figures for the manuscript. All authors have reviewed the manuscript.

Funding This research was funded by a grant from the Russian Science Foundation (grant No 21-72-10157, rscf.ru/project/21-72-10157).

Data Availability All SDO/AIA data used in this work are courtesy of NASA/SDO and AIA science team and are available from the JSOC (jsoc.stanford.edu) without restriction.

Declarations

Competing interests The authors declare no competing interests.

References

- Andretta, V., Del Zanna, G., Jordan, S.D.: 2003, The EUV helium spectrum in the quiet Sun: a by-product of coronal emission? *Astron. Astrophys.* **400**, 737. DOI. ADS.
- Andretta, V., Telloni, D., Del Zanna, G.: 2012, Coronal diagnostics from narrowband images around 30.4 nm. *Solar Phys.* **279**, 53. DOI. ADS.
- Asplund, M., Grevesse, N., Sauval, A.J., Scott, P.: 2009, The chemical composition of the Sun. *Annu. Rev. Astron. Astrophys.* **47**, 481. DOI. ADS.
- Avrett, E.H., Loeser, R.: 2008, Models of the solar chromosphere and transition region from SUMER and HRTS observations: formation of the extreme-ultraviolet spectrum of hydrogen, carbon, and oxygen. *Astron. Astrophys. Suppl. Ser.* **175**, 229. DOI. ADS.

- Bai, X., Tian, H., Deng, Y., Wang, Z., Yang, J., Zhang, X., Zhang, Y., Qi, R., Wang, N., Gao, Y., Yu, J., He, C., Shen, Z., Shen, L., Guo, S., Hou, Z., Ji, K., Bi, X., Duan, W., Yang, X., Lin, J., Hu, Z., Song, Q., Yang, Z., Chen, Y., Qiao, W., Ge, W., Li, F., Jin, L., He, J., Chen, X., Zhu, X., He, J., Shi, Q., Liu, L., Li, J., Xu, D., Liu, R., Li, T., Feng, Z., Wang, Y., Fan, C., Liu, S., Guo, S., Sun, Z., Wu, Y., Li, H., Yang, Q., Ye, Y., Gu, W., Wu, J., Zhang, Z., Yu, Y., Ye, Z., Sheng, P., Wang, Y., Li, W., Huang, Q., Zhang, Z.: 2023, The solar upper transition region imager (SUTRI) onboard the SATech-01 satellite. *Res. Astron. Astrophys.* **23**, 065014. DOI. ADS.
- Boerner, P., Edwards, C., Lemen, J., Rausch, A., Schrijver, C., Shine, R., Shing, L., Stern, R., Tarbell, T., Title, A., Wolfson, C.J., Soufli, R., Spiller, E., Gullikson, E., McKenzie, D., Windt, D., Golub, L., Podgorski, W., Testa, P., Weber, M.: 2012, Initial calibration of the atmospheric imaging assembly (AIA) on the solar dynamics observatory (SDO). *Solar Phys.* **275**, 41. DOI. ADS.
- Boerner, P.F., Testa, P., Warren, H., Weber, M.A., Schrijver, C.J.: 2014, Photometric and thermal cross-calibration of solar EUV instruments. *Solar Phys.* **289**, 2377. DOI. ADS.
- Bogachev, S.A., Ulyanov, A.S., Kirichenko, A.S., Loboda, I.P., Reva, A.A.: 2020, Microflares and nanoflares in the solar corona. *Phys. Usp.* **63**, 783. DOI. ADS.
- Bogachev, S.A., Loboda, I.P., Reva, A.A., Ulyanov, A.S., Kirichenko, A.S.: 2022, Difference in the characteristics of solar macrospicules at low and high latitudes. *Astron. Lett.* **48**, 47. DOI. ADS.
- Cheung, M.C.M., Boerner, P., Schrijver, C.J., Testa, P., Chen, F., Peter, H., Malanushenko, A.: 2015, Thermal diagnostics with the atmospheric imaging assembly on board the solar dynamics observatory: a validated method for differential emission measure inversions. *Astrophys. J.* **807**, 143. DOI. ADS.
- Cushman, G.W., Rense, W.A.: 1978, Solar He II (304 Å) and Si XI (303 Å) line profiles. *Solar Phys.* **58**, 299. DOI. ADS.
- David, C., Gabriel, A.H., Bely-Dubau, F., Fludra, A., Lemaire, P., Wilhelm, K.: 1998, Measurement of the electron temperature gradient in a solar coronal hole. *Astron. Astrophys.* **336**, L90. ADS.
- DeForest, C.E., Hoeksema, J.T., Gurman, J.B., Thompson, B.J., Plunkett, S.P., Howard, R., Harrison, R.C., Hasslerz, D.M.: 1997, Polar plume anatomy: results of a coordinated observation. *Solar Phys.* **175**, 393. DOI. ADS.
- Del Zanna, G., Andretta, V.: 2011, The EUV spectrum of the Sun: SOHO CDS NIS irradiances from 1998 until 2010. *Astron. Astrophys.* **528**, A139. DOI. ADS.
- Del Zanna, G., Wieman, S.R., Andretta, V., Didkovsky, L.: 2015, The EUV spectrum of the Sun: SOHO, SEM, and CDS irradiances. *Astron. Astrophys.* **581**, A25. DOI. ADS.
- Del Zanna, G., Storey, P.J., Badnell, N.R., Andretta, V.: 2020, Helium line emissivities in the solar corona. *Astrophys. J.* **898**, 72. DOI. ADS.
- Del Zanna, G., Dere, K.P., Young, P.R., Landi, E.: 2021, CHIANTI—an atomic database for emission lines. XVI. Version 10, further extensions. *Astrophys. J.* **909**, 38. DOI. ADS.
- Delaboudinière, J.-P., Artzner, G.E., Brunaud, J., Gabriel, A.H., Hochedez, J.F., Millier, F., Song, X.Y., Au, B., Dere, K.P., Howard, R.A., Kreplin, R., Michels, D.J., Moses, J.D., Defise, J.M., Jamar, C., Rochus, P., Chauvineau, J.P., Marioge, J.P., Catura, R.C., Lemen, J.R., Shing, L., Stern, R.A., Gurman, J.B., Neupert, W.M., Maucherat, A., Clette, F., Cugnon, P., Van Dessel, E.L.: 1995, EIT: extreme-ultraviolet imaging telescope for the SOHO mission. *Solar Phys.* **162**, 291. DOI. ADS.
- Domingo, V., Fleck, B., Poland, A.I.: 1995, The SOHO mission: an overview. *Solar Phys.* **162**, 1. DOI. ADS.
- Feldman, U., Laming, J.M.: 2000, Element abundances in the upper atmospheres of the Sun and stars: update of observational results. *Phys. Scr.* **61**, 222. DOI. ADS.
- Feldman, U., Mandelbaum, P., Seely, J.F., Doschek, G.A., Gursky, H.: 1992, The potential for plasma diagnostics from stellar extreme-ultraviolet observations. *Astron. Astrophys. Suppl. Ser.* **81**, 387. DOI. ADS.
- Fludra, A., Schmelz, J.T.: 1999, The absolute coronal abundances of sulfur, calcium, and iron from Yohkoh-BCS flare spectra. *Astron. Astrophys.* **348**, 286. ADS.
- Golding, T.P., Leenaerts, J., Carlsson, M.: 2017, Formation of the helium extreme-UV resonance lines. *Astron. Astrophys.* **597**, A102. DOI. ADS.
- Golub, L., DeLuca, E., Austin, G., Bookbinder, J., Caldwell, D., Cheimets, P., Cirtain, J., Cosmo, M., Reid, P., Sette, A., Weber, M., Sakao, T., Kano, R., Shibusaki, K., Hara, H., Tsuneta, S., Kumagai, K., Tamura, T., Shimojo, M., McCracken, J., Carpenter, J., Haight, H., Siler, R., Wright, E., Tucker, J., Rutledge, H., Barbera, M., Peres, G., Varisco, S.: 2007, The X-ray telescope (XRT) for the Hinode mission. *Solar Phys.* **243**, 63. DOI. ADS.
- Grevesse, N., Asplund, M., Sauval, A.J.: 2007, The solar chemical composition. *Space Sci. Rev.* **130**, 105. DOI. ADS.
- Harrison, R.A., Sawyer, E.C., Carter, M.K., Cruise, A.M., Cutler, R.M., Fludra, A., Hayes, R.W., Kent, B.J., Lang, J., Parker, D.J., Payne, J., Pike, C.D., Peskett, S.C., Richards, A.G., Gulhane, J.L., Norman, K., Breeveld, A.A., Breeveld, E.R., Al Janabi, K.F., Mccalden, A.J., Parkinson, J.H., Self, D.G., Thomas, P.D., Poland, A.I., Thomas, R.J., Thompson, W.T., Kjeldseth-Moe, O., Brekke, P., Karud, J., Maltby, P., Aschenbach, B., Bräuning, H., Kühne, M., Hollandt, J., Siegmund, O.H.W., Huber, M.C.E., Gabriel,

- A.H., Mason, H.E., Bromage, B.J.I.: 1995, The coronal diagnostic spectrometer for the solar and heliospheric observatory. *Solar Phys.* **162**, 233. DOI. ADS.
- Holman, G.D.: 2016, Scientific considerations for future spectroscopic measurements from space of activity on the Sun. *J. Geophys. Res. Space Phys.* **121**, 11667. DOI. ADS.
- Jordan, S.D., Thompson, W.T., Thomas, R.J., Neupert, W.M.: 1993, Solar coronal observations and formation of the He II 304 Angstrom line. *Astrophys. J.* **406**, 346. DOI. ADS.
- Joulin, V., Buchlin, E., Solomon, J., Guennou, C.: 2016, Energetic characterisation and statistics of solar coronal brightenings. *Astron. Astrophys.* **591**, A148. DOI. ADS.
- Kirichenko, A.S., Bogachev, S.A.: 2017, The relation between magnetic fields and X-ray emission for solar microflares and active regions. *Solar Phys.* **292**, 120. DOI. ADS.
- Kirichenko, A., Kuzin, S., Shestov, S., Ulyanov, A., Pertsov, A., Bogachev, S., Reva, A., Loboda, I., Vishnyakov, E., Dyatkov, S., Erkhova, N., Steślicki, M., Sylwester, J., Plocieniak, S., Podgórski, P., Kowaliński, M., Bakala, J., Szaforz, Ż., Siarkowski, M., Ścisłowski, D., Mrozek, T., Sylwester, B., Malyshev, I., Pestov, A., Polkovnikov, V., Toropov, M., Salashchenko, N., Tsybin, N., Sychkhalo, N.: 2021, KORTES mission for solar activity monitoring onboard international space station. *Front. Astron. Space Sci.* **8**, 66. DOI. ADS.
- Kiss, T.S., Erdélyi, R.: 2018, On quasi-biennial oscillations in chromospheric macrospicules and their potential relation to the global solar magnetic field. *Astrophys. J.* **857**, 113. DOI. ADS.
- Kiss, T.S., Gyenge, N., Erdélyi, R.: 2017, Systematic variations of macrospicule properties observed by SDO/AIA over half a decade. *Astrophys. J.* **835**, 47. DOI. ADS.
- Kosugi, T., Matsuzaki, K., Sakao, T., Shimizu, T., Sone, Y., Tachikawa, S., Hashimoto, T., Minesugi, K., Ohnishi, A., Yamada, T., Tsuneta, S., Hara, H., Ichimoto, K., Suematsu, Y., Shimojo, M., Watanabe, T., Shimada, S., Davis, J.M., Hill, L.D., Owens, J.K., Title, A.M., Culhane, J.L., Harra, L.K., Doschek, G.A., Golub, L.: 2007, The Hinode (solar-b) mission: an overview. *Solar Phys.* **243**, 3. DOI. ADS.
- Kumar, P., Karpen, J.T., Antiochos, S.K., Wyper, P.F., DeVore, C.R., DeForest, C.E.: 2019, Multiwavelength study of equatorial coronal-hole jets. *Astrophys. J.* **873**, 93. DOI. ADS.
- Kuzin, S.V., Bogachev, S.A., Zhitnik, I.A., Pertsov, A.A., Ignatiev, A.P., Mitrofanov, A.M., Slemzin, V.A., Shestov, S.V., Sukhodrev, N.K., Bugaenko, O.I.: 2009, TESIS experiment on EUV imaging spectroscopy of the Sun. *Adv. Space Res.* **43**, 1001. DOI. ADS.
- Kuzin, S.V., Bogachev, S.A., Pertsov, A.A., Shestov, S.V., Reva, A.A., Ulyanov, A.S.: 2011, EUV observations of the solar corona with superhigh spatial resolution in the ARCA project. *Bull. Russ. Acad. Sci., Phys.* **75**, 87. DOI. ADS.
- Labrosse, N., Dalla, S., Marshall, S.: 2010, Automatic detection of limb prominences in 304 Å EUV images. *Solar Phys.* **262**, 449. DOI. ADS.
- Labrosse, N., Gouttebroze, P.: 2001, Formation of helium spectrum in solar quiescent prominences. *Astron. Astrophys.* **380**, 323. DOI. ADS.
- Landi, E., Feldman, U., Dere, K.P.: 2002, CHIANTI-an atomic database for emission lines. V. Comparison with an isothermal spectrum observed with SUMER. *Astron. Astrophys. Suppl. Ser.* **139**, 281. DOI. ADS.
- Lemen, J.R., Title, A.M., Akin, D.J., Boerner, P.F., Chou, C., Drake, J.F., Duncan, D.W., Edwards, C.G., Friedlaender, F.M., Heyman, G.F., Hurlburt, N.E., Katz, N.L., Kushner, G.D., Levay, M., Lindgren, R.W., Mathur, D.P., McFeaters, E.L., Mitchell, S., Rehse, R.A., Schrijver, C.J., Springer, L.A., Stern, R.A., Tarbell, T.D., Wuelser, J.-P., Wolfson, C.J., Yanari, C., Bookbinder, J.A., Cheimets, P.N., Caldwell, D., Deluca, E.E., Gates, R., Golub, L., Park, S., Podgorski, W.A., Bush, R.I., Scherrer, P.H., Gummin, M.A., Smith, P., Auker, G., Jerram, P., Pool, P., Soufli, R., Windt, D.L., Beardsley, S., Clapp, M., Lang, J., Waltham, N.: 2012, The atmospheric imaging assembly (AIA) on the solar dynamics observatory (SDO). *Solar Phys.* **275**, 17. DOI. ADS.
- Liu, J., Song, A., Jess, D.B., Zhang, J., Mathioudakis, M., Soós, S., Keenan, F.P., Wang, Y., Erdélyi, R.: 2023, Power-law distribution of solar cycle-modulated coronal jets. *Astron. Astrophys. Suppl. Ser.* **266**, 17. DOI. ADS.
- Loboda, I.P., Bogachev, S.A.: 2015, Quiescent and eruptive prominences at solar minimum: a statistical study via an automated tracking system. *Solar Phys.* **290**, 1963. DOI. ADS.
- Loboda, I.P., Bogachev, S.A.: 2017, Plasma dynamics in solar macrospicules from high-cadence extreme-UV observations. *Astron. Astrophys.* **597**, A78. DOI. ADS.
- Loboda, I.P., Bogachev, S.A.: 2019, What is a macrospicule? *Astrophys. J.* **871**, 230. DOI. ADS.
- Lodders, K., Palme, H., Gail, H.-P.: 2009, Abundances of the elements in the solar system. In: *Landolt Börnstein* **4B**, 712. DOI. ADS.
- Mierla, M., Zhukov, A.N., Berghmans, D., Parenti, S., Auchère, F., Heinzel, P., Seaton, D.B., Palmerio, E., Jejič, S., Janssens, J., Kraaikamp, E., Nicula, B., Long, D.M., Hayes, L.A., Jebaraj, I.C., Talpeanu, D.-C., D'Huys, E., Dolla, L., Gissot, S., Magdalenic, J., Rodriguez, L., Shestov, S., Stegen, K., Verbeeck, C., Sasso, C., Romoli, M., Andretta, V.: 2022, Prominence eruption observed in He II 304 Å up to $> 6R_{\odot}$ by EUV/FSI aboard Solar Orbiter. *Astron. Astrophys.* **662**, L5. DOI. ADS.

- Müller, D., St. Cyr, O.C., Zouganelis, I., Gilbert, H.R., Marsden, R., Nieves-Chinchilla, T., Antonucci, E., Auchère, F., Berghmans, D., Horbury, T.S., Howard, R.A., Krucker, S., Maksimovic, M., Owen, C.J., Rochus, P., Rodriguez-Pacheco, J., Romoli, M., Solanki, S.K., Bruno, R., Carlsson, M., Fludra, A., Harra, L., Hassler, D.M., Livi, S., Louarn, P., Peter, H., Schühle, U., Teriaca, L., del Toro Iniesta, J.C., Wimmer-Schweingruber, R.F., Marsch, E., Velli, M., De Groof, A., Walsh, A., Williams, D.: 2020, The Solar Orbiter mission. Science overview. *Astron. Astrophys.* **642**, A1. DOI. ADS.
- Parker, J.D., Kankelborg, C.C.: 2022, Determining the spectral content of MOSES images. *Astrophys. J.* **932**, 130. DOI. ADS.
- Pascoe, D.J., Smyrli, A., Van Doorselaere, T.: 2019, Coronal density and temperature profiles calculated by forward modeling EUV emission observed by SDO/AIA. *Astrophys. J.* **884**, 43. DOI. ADS.
- Pereira, T.M.D., De Pontieu, B., Carlsson, M.: 2012, Quantifying spicules. *Astrophys. J.* **759**, 18. DOI. ADS.
- Pesnell, W.D., Thompson, B.J., Chamberlin, P.C.: 2012, The solar dynamics observatory (SDO). *Solar Phys.* **275**, 3. DOI. ADS.
- Pietarila, A., Judge, P.G.: 2004, On the formation of the resonance lines of helium in the Sun. *Astrophys. J.* **606**, 1239. DOI. ADS.
- Poduval, B., DeForest, C.E., Schmelz, J.T., Pathak, S.: 2013, Point-spread functions for the extreme-ultraviolet channels of SDO/AIA telescopes. *Astrophys. J.* **765**, 144. DOI. ADS.
- Pucci, S., Poletto, G., Sterling, A.C., Romoli, M.: 2013, Physical parameters of standard and blowout jets. *Astrophys. J.* **776**, 16. DOI. ADS.
- Reva, A.A., Ulyanov, A.S., Kuzin, S.V.: 2016, Current sheet structures observed by the TESIS EUV telescope during a flux rope eruption on the Sun. *Astrophys. J.* **832**, 16. DOI. ADS.
- Reva, A.A., Ulyanov, A.S., Shestov, S.V., Kuzin, S.V.: 2016, Breakout reconnection observed by the TESIS EUV telescope. *Astrophys. J.* **816**, 90. DOI. ADS.
- Reva, A.A., Kirichenko, A.S., Ulyanov, A.S., Kuzin, S.V.: 2017, Observations of the coronal mass ejection with a complex acceleration profile. *Astrophys. J.* **851**, 108. DOI. ADS.
- Rochus, P., Auchère, F., Berghmans, D., Harra, L., Schmutz, W., Schühle, U., Addison, P., Appourchaux, T., Aznar Cuadrado, R., Baker, D., Barbay, J., Bates, D., BenMoussa, A., Bergmann, M., Beurthe, C., Borge, B., Bonte, K., Bouzit, M., Bradley, L., Büchel, V., Buchlin, E., Büchner, J., Cabé, F., Cadiergues, L., Chaigneau, M., Chares, B., Choque Cortez, C., Coker, P., Condamine, M., Coumar, S., Curdt, W., Cutler, J., Davies, D., Davison, G., Defise, J.-M., Del Zanna, G., Delmotte, F., Delouille, V., Dolla, L., Dumesnil, C., Dürig, F., Enge, R., François, S., Fourmond, J.-J., Gillis, J.-M., Giordanengo, B., Gissot, S., Green, L.M., Guerreiro, N., Guilbaud, A., Gyo, M., Haberreiter, M., Hafiz, A., Hailey, M., Halain, J.-P., Hansotte, J., Hecquet, C., Heerlein, K., Hellin, M.-L., Hemsley, S., Hermans, A., Hervier, V., Hochedez, J.-F., Houbrechts, Y., Ihsan, K., Jacques, L., Jérôme, A., Jones, J., Kahle, M., Kennedy, T., Klapproth, M., Kolleck, M., Koller, S., Kotsialos, E., Kraaikamp, E., Langer, P., Lawrenson, A., Le Clech', J.-C., Lenaerts, C., Liebecq, S., Linder, D., Long, D.M., Mampaey, B., Markiewicz-Innes, D., Marquet, B., Marsch, E., Matthews, S., Mazy, E., Mazzoli, A., Meining, S., Meltchakov, E., Mercier, R., Meyer, S., Monecke, M., Monfort, F., Morinaud, G., Moron, F., Mountney, L., Müller, R., Nicula, B., Parenti, S., Peter, H., Pfflner, D., Philippon, A., Phillips, I., Plessier, J.-Y., Pilyser, E., Rabecki, F., Ravet-Krill, M.-F., Rebellato, J., Renotte, E., Rodriguez, L., Roose, S., Rosin, J., Rossi, L., Roth, P., Roussel, F., Roulliy, M., Rousseau, A., Ruane, K., Scanlan, J., Schlatter, P., Seaton, D.B., Silliman, K., Smit, S., Smith, P.J., Solanki, S.K., Spescha, M., Spencer, A., Stegen, K., Stockman, Y., Szwec, N., Tamiatto, C., Tandy, J., Teriaca, L., Theobald, C., Tychon, I., van Driel-Gesztelyi, L., Verbeeck, C., Vial, J.-C., Werner, S., West, M.J., Westwood, D., Wiegelmann, T., Willis, G., Winter, B., Zerr, A., Zhang, X., Zhukov, A.N.: 2020, The solar orbiter EUV instrument: the extreme ultraviolet imager. *Astron. Astrophys.* **642**, A8. DOI. ADS.
- Schmelz, J.T., Reames, D.V., von Steiger, R., Basu, S.: 2012, Composition of the solar corona, solar wind, and solar energetic particles. *Astrophys. J.* **755**, 33. DOI. ADS.
- Seaton, D.B., Darnel, J.M.: 2018, Observations of an eruptive solar flare in the extended EUV solar corona. *Astrophys. J. Lett.* **852**, L9. DOI. ADS.
- Tadikonda, S.K., Freesland, D.C., Minor, R.R., Seaton, D.B., Comeyne, G.J., Krimchansky, A.: 2019, Coronal imaging with the solar UltraViolet imager. *Solar Phys.* **294**, 28. DOI. ADS.
- Thomas, R.J., Neupert, W.M.: 1994, Extreme ultraviolet spectrum of a solar active region from SERTS. *Astrophys. J. Suppl. Ser.* **91**, 461. DOI. ADS.
- Thompson, W.T., Brekke, P.: 2000, EUV full-sun imaged spectral atlas using the SOHO coronal diagnostic spectrometer. *Solar Phys.* **195**, 45. DOI. ADS.
- Ulyanov, A.S., Bogachev, S.A., Loboda, I.P., Reva, A.A., Kirichenko, A.S.: 2019, Direct evidence for magnetic reconnection in a solar EUV nanoflare. *Solar Phys.* **294**, 128. DOI. ADS.
- Vernazza, J.E., Avrett, E.H., Loeser, R.: 1981, Structure of the solar chromosphere. III. Models of the EUV brightness components of the quiet sun. *Astrophys. J. Suppl. Ser.* **45**, 635. DOI. ADS.

- Warren, H.P., Brooks, D.H.: 2009, The temperature and density structure of the solar corona. I. observations of the quiet sun with the EUV imaging spectrometer on hinode. *Astrophys. J.* **700**, 762. DOI. ADS.
- Wilhelm, K., Marsch, E., Dwivedi, B.N., Hassler, D.M., Lemaire, P., Gabriel, A.H., Huber, M.C.E.: 1998, The solar corona above polar coronal holes as seen by SUMER on SOHO. *Astrophys. J.* **500**, 1023. DOI. ADS.
- Woods, T.N., Eparvier, F.G., Hock, R., Jones, A.R., Woodraska, D., Judge, D., Didkovsky, L., Lean, J., Mariska, J., Warren, H., McMullin, D., Chamberlin, P., Berthiaume, G., Bailey, S., Fuller-Rowell, T., Sojka, J., Tobiska, W.K., Viereck, R.: 2012, Extreme ultraviolet variability experiment (EVE) on the solar dynamics observatory (SDO): overview of science objectives, instrument design, data products, and model developments. *Solar Phys.* **275**, 115. DOI. ADS.
- Wuelser, J.-P., Lemen, J.R., Tarbell, T.D., Wolfson, C.J., Cannon, J.C., Carpenter, B.A., Duncan, D.W., Gradwohl, G.S., Meyer, S.B., Moore, A.S., Navarro, R.L., Pearson, J.D., Rossi, G.R., Springer, L.A., Howard, R.A., Moses, J.D., Newmark, J.S., Delaboudiniere, J.-P., Artzner, G.E., Auchere, F., Bougnet, M., Bouyries, P., Bridou, F., Clotaire, J.-Y., Colas, G., Delmotte, F., Jerome, A., Lamare, M., Mercier, R., Mullet, M., Ravet, M.-F., Song, X., Bothmer, V., Deutsch, W.: 2004, EUVI: the STEREO-SECCHI extreme ultraviolet imager. In: Fineschi, S., Gummin, M.A. (eds.) *Telescopes and Instrumentation for Solar Astrophysics, Proc. Soc. Photo-Opt. Instrum. Eng. (SPIE)* **CS-5171**, 111. DOI. ADS.

Publisher's Note Springer Nature remains neutral with regard to jurisdictional claims in published maps and institutional affiliations.

Springer Nature or its licensor (e.g. a society or other partner) holds exclusive rights to this article under a publishing agreement with the author(s) or other rightsholder(s); author self-archiving of the accepted manuscript version of this article is solely governed by the terms of such publishing agreement and applicable law.